PROCEEDINGS OF SCIENCE

General characteristics of pp collisions at LHC

L. Bravina[*], **E. Zabrodin**
Department of Physics, University of Oslo, Oslo, Norway
E-mail: larissa.bravina@fys.uio.no

J. Bleibel, C. Fuchs
Institute for Theoretical Physics, University of Tuebingen, Tuebingen, Germany

A. Kaidalov
Institute for Theoretical and Experimental Physics, Moscow, Russia

The quark-gluon string model is employed to study bulk production of hadrons and their spectra in inelastic pp collisions at ultrarelativistic energies. Good agreement with the available experimental data is obtained and predictions are made for pp collisions at full LHC energy $\sqrt{s} = 14$ TeV. Fulfillment of scaling trends is checked both at midrapidity and in fragmentation regions. Feynman scaling and extended longitudinal scaling are found to hold in the fragmentation regions only.

High-pT Physics at LHC -09
February 4- 4 2009
Prague, Czech Republic

[*]Speaker.

PoS(High-pT physics09)010

1. Introduction

The experiments with proton-proton collisions at CERN Large Hadron Collider (LHC) are planned to span the center-of-mass energies from $\sqrt{s} = 900$ GeV to $\sqrt{s} = 14$ TeV, thus entering the completely new domain of accelerator's high energy physics. Still, even the top LHC energy is not high enough to allow for description of the processes solely within the framework of perturbative quantum chromodynamics (pQCD). Many of partonic interactions should proceed at large distances or, equivalently, with small momentum transfer. The running coupling constant α_S in such soft interactions is close to unity, and one has to rely on available non-perturbative approaches. In the present paper we apply the quark-gluon string model (QGSM) [1], namely, its Monte Carlo version [2] that permits the treatment of both soft and hard partonic processes on a same footing. Our main goal is to make predictions for yields and spectra of charged particles in pp interactions at $\sqrt{s} = 14$ TeV. The paper is organized as follows. After the description of basic principles of the QGSM in Sect. 2, the model results are confronted in Sect. 3 with the experimental data on bulk particle production, taken from $\sqrt{s} = 200$ GeV up to $\sqrt{s} = 1800$ GeV. From this comparison one can see that the model adequately reproduces the data. Predictions for pp collisions at $\sqrt{s} = 14$ TeV are made in Sect. 3 as well. Of special interest are the scaling trends, predicted and partially observed in elementary reactions at energies up to $\sqrt{s} = 1.8$ TeV. The most famous is the Feynman scaling hypothesis [3]. As shown in Sect. 3, the QGSM unambiguously supports the fulfillment of Feynman scaling only in fragmentation region $x_F > 0.2$, whereas strong violation of the scaling is observed at midrapidity. Conclusions are drawn in Sec. 4.

2. Quark-Gluon String Model

The QGSM [1] is based on Gribov Reggeon Field Theory [4] and employs the $1/N$ series expansion of the amplitude for process in QCD, where N can be number of colors N_c [5] or number of flavors N_f [6]. The method is also called the topological expansion method, because here the amplitude of a hadronic process is represented as a sum of diagrams of various topologies. It may be shown (see, e.g. [6, 8]) that these diagrams are similar to processes describing the exchange of Regge singularities in the t-channel. Two main classes of the diagrams, planar diagrams (with the exchange of quantum numbers) and cylinder diagrams (without the quantum number exchange), correspond to exchange of Reggeons and Pomerons, respectively. To find the amplitude of multiparticle process one has to cut the diagrams in the s-channel. From here the physical picture of quark-gluon strings arises. The variety of diagrams is rich [2], but the so-called preasymptotic diagrams are important at low and intermediate energies only. They can be disregarded at $p_{lab} \geq 100$ GeV/c, because their contribution to the total cross section drops as $s^{-1/2}$. As a result, just few inelastic diagrams shown in Fig. 1 survive at ultrarelativistic energies for pp collisions, namely, the cylinder diagram corresponding to the multi-chain process [Fig. 1(a)], triple-Reggeon and triple-Pomeron diagrams representing the diffractive process with small-mass [Fig. 1(b)] and large-mass [Fig. 1(c)] excitation, respectively, and double-diffractive diagram [Fig. 1(d)]. The statistical weight of each subprocess is expressed in terms of the interaction cross section for the given subprocess $\sigma_i(s)$

$$\omega_i = \sigma_i(s)/\sigma_{inel}(s) \ . \tag{2.1}$$

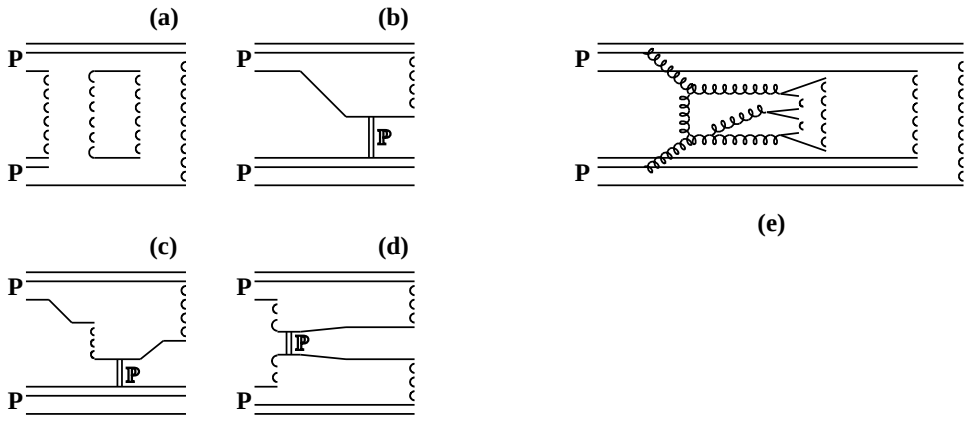

Figure 1: Diagrams of particle production processes included in the modeling of pp interactions at ultrarelativistic energies. See text for details.

Then, the hadron inelastic interaction cross section $\sigma_{inel}(s) = \sigma_{tot}(s) - \sigma_{el}(s)$ is split into the cross section for single diffractive interactions $\sigma_{SD}(s)$ and the cross section for non-diffractive reactions $\sigma_{ND}(s)$, as it is usually done in analysis of experimental data. Experimental parameterizations are used to determine the total hadron interaction cross section $\sigma_{tot}(s)$ and the elastic interaction cross section $\sigma_{el}(s)$. The inelastic non-diffractive interaction cross section $\sigma_{ND}(s)$ can be expressed via the sum of the cross sections for the production of $n = 1,2,\ldots$ pairs of quark-gluon strings, or cut Pomerons, and the cross section of double diffractive process

$$\sigma_{ND}(s) = \sum_{n=1}^{\infty} \sigma_n(s) + \sigma_{DD}(s) \ . \tag{2.2}$$

To find $\sigma_n(s)$ one can rely on the eikonal model [7] which states that

$$\sigma_n(s) = \frac{\sigma_P}{nz}\left(1 - \exp(-z)\sum_{k=0}^{n-1}\frac{z^k}{k!}\right) \ , \ k \geq 1 \ . \tag{2.3}$$

Here

$$\sigma_P \ = \ 8\pi\gamma_P \exp(\Delta\xi) \ , \tag{2.4}$$

$$z \ = \ \frac{2C\gamma_P}{(R_P^2 + \alpha'_P\xi)} \exp(\Delta\xi) \ . \tag{2.5}$$

The parameters γ_P and R_P are Pomeron-nucleon vertex parameters, quantity $\Delta \equiv \alpha_P(0) - 1$, and $\alpha_P(0)$ and α'_P is the intercept and the slope of the Pomeron trajectory, respectively. The quantity C takes into account the deviation from the pure eikonal approximation $(C = 1)$ due to intermediate inelastic diffractive states, $\xi = \ln(s/s_0)$ and s_0 is a scale parameter.

To take into account the jet formation and describe simultaneously the increase of the total and inelastic hadronic interaction cross section with rising $\sqrt{s}$ the eikonal model was properly modified

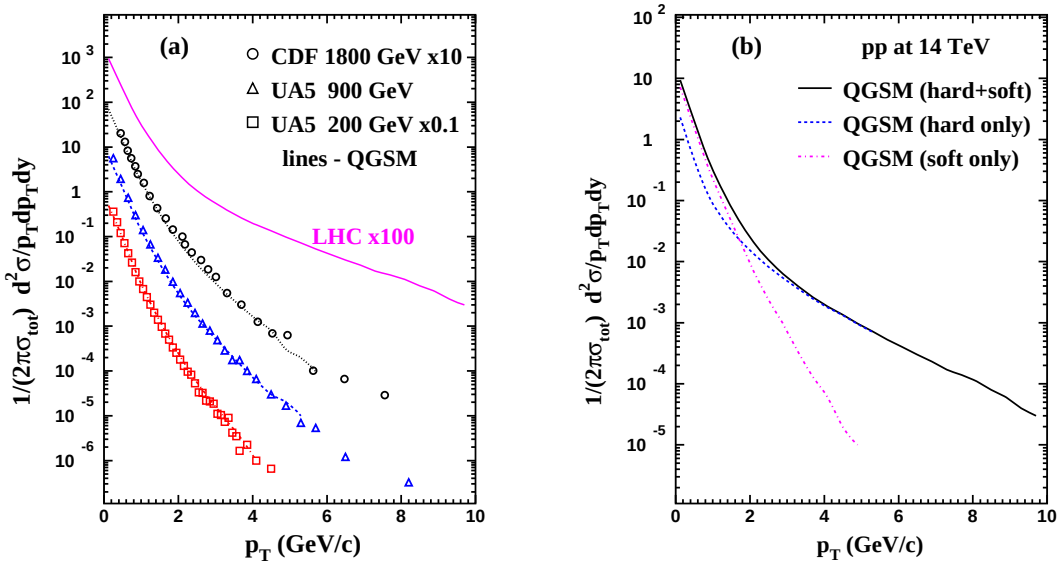

Figure 2: (a) Transverse momentum distributions of the invariant cross section in pp collisions for all energies in question. (b) Soft, hard and combined contributions to p_T spectrum in pp collisions at $\sqrt{s} =$ 1.8 TeV. Experimental data for $\bar{p}p$ reactions are taken from [11] and [12].

in [9] by introducing the new term that represents the hard Pomeron exchange. The cut of the hard Pomeron leads to formation of two hadronic jets, see Fig. 1(e), where the string formation in hard gluon-gluon scattering and soft Pomeron exchange in proton-proton collision is displayed.

There is no unique theoretical prescription for modeling the fragmentation of a string with a given mass, momentum and quark content into hadrons. In the presented version of the QGSM the Field-Feynman algorithm [10] is employed. It enables one to consider emission of hadrons from both ends of the string with equal probabilities. The break-up procedure invokes the energy-momentum conservation and the preservation of the quark numbers. The transverse momentum of the (di)quarks in the vacuum pair is determined by the power-law probability

$$f(p_T^2)\,dp_T^2 = \frac{3Db_2(s)}{\pi(1+Dp_T^2)^4}\,dp_T^2\,, \tag{2.6}$$

$$b_2(s) = 0.33 + 0.016\ln s\,, \tag{2.7}$$

with $D = 0.34\,(\mathrm{GeV}/c)^{-2}$. Details of the theoretical description of the QGSM and its Monte Carlo realization can be found in [1, 2].

3. Yields and spectra. Comparison with data and predictions for LHC

We used experimental data obtained by the UA5 Collaboration for proton - antiproton collisions at c.m. energies $\sqrt{s} = 200$ GeV, 546 GeV and 900 GeV [11], and by the CDF Collaboration for $\bar{p}p$ collisions at $\sqrt{s} = 1800$ GeV [12, 13]. At such high energies the annihilation cross section is almost zero and the main characteristics of particle production in pp and $\bar{p}p$ interactions are essentially similar. The transverse momentum distributions of the invariant cross section $E\dfrac{d^3\sigma}{dp^3}$

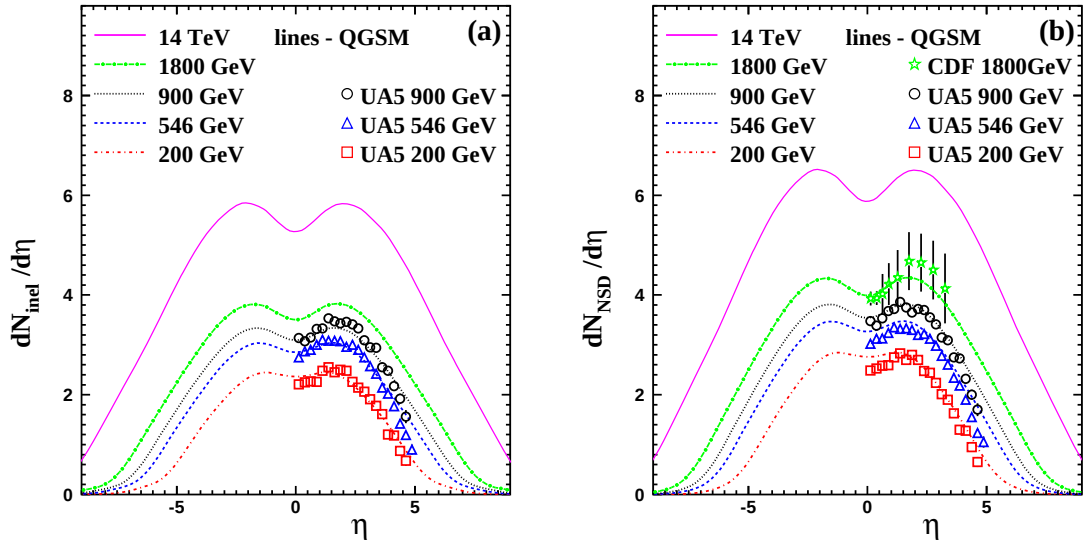

Figure 3: The charged particle pseudorapidity spectra for (a) inelastic and (b) non-single-diffractive events calculated in QGSM in comparison with the $\bar{p}p$ data at $\sqrt{s} = 200$ GeV, 546 GeV, 900 GeV and 1.8 TeV. Data are taken from [11] and [12].

divided to σ_{tot} are presented in Fig. 2(left) for all energies in question. We see that the QGSM reproduces the experimental data pretty well. To study the interplay between the soft and hard processes we show separately their fractional contributions and combined results for pp collisions at top LHC energy $\sqrt{s} = 14$ TeV in Fig. 2(right). One can see that the soft processes dominate at $p_T \leq 2$ GeV/c, whereas at higher transverse momenta the major contribution to the cross section comes from the minijets.

The charged particle pseudorapidity spectra $\frac{1}{\sigma_{inel}}\frac{d\sigma_{inel}}{d\eta}$ and $\frac{1}{\sigma_{NSD}}\frac{d\sigma_{NSD}}{d\eta}$ for inelastic and non-single-diffractive events, respectively, are displayed in Fig. 3 together with the $\bar{p}p$ data at $\sqrt{s} = 200$ GeV, 546 GeV, 900 GeV and 1.8 TeV. QGSM predictions for $\sqrt{s} = 14$ TeV are plotted here also. The model gives good description of these distributions within the indicated energy range except, maybe, not very distinct dip at midrapidity for two lower energies, $\sqrt{s} = 200$ GeV and 546 GeV. For pp collisions at top LHC energy QGSM predicts further increase of the central particle densities to

$$\frac{dN_{inel}}{d\eta}|_{\eta=0} = 5.3 \quad , \quad \frac{dN_{NSD}}{d\eta}|_{\eta=0} = 5.9 \ .$$

Compared to the Tevatron, the rise of the central particle density at LHC is expected to be about 50%.

Let us briefly recall the main assumptions and predictions of the hypothesis of Feynman scaling [3]. It requires scaling behavior of particle spectra within the whole kinematically allowed region of the Feynman scaling variable $x_F \equiv p_{||}/p_{||}^{max}$ or, alternatively, c.m. rapidity y^* at ultrarelativistic energies $s \to \infty$. In addition, the existence of non-vanishing central area $|x_F| \leq x_0$, $x_0 \sim 0.1 - 0.2$ is postulated. In terms of rapidity this central region increases with rising $\sqrt{s}$ as

$$(\Delta y^*)_{centr} \approx 2 \ln \left[x_0 \sqrt{s}/m_T\right] \tag{3.1}$$

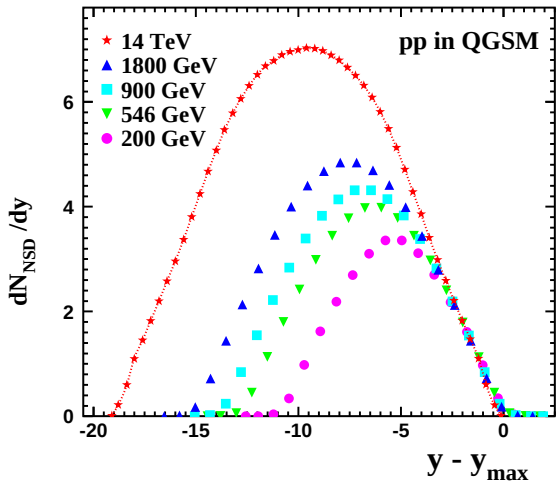

Figure 4: The distributions $\frac{1}{\sigma_{NSD}}\frac{d\sigma_{NSD}}{dy}$ as functions of rapidity difference $y-y_{max}$ obtained in QGSM for energies $\sqrt{s}=200$ GeV, 546 GeV, 900 GeV, 1.8 TeV and 14 TeV.

provided the transverse mass $m_T=\sqrt{m_0^2+p_T^2}$ is finite. In contrast, the fragmentation region remains constant

$$(\Delta y^*)_{frag}\approx \ln(1/x_0)\ . \tag{3.2}$$

From here it follows that (i) in the central area the particle density $\rho_{cent}(y^*,p_T,s)$ depends on neither y^* nor $\sqrt{s}$, i.e. $\rho_{cent}\equiv\rho_{cent}(p_T)$, and rapidity spectra of particles have, therefore, a broad plateau; (ii) this area gives a main contribution to average multiplicity of produced hadrons; (iii) contribution to the average multiplicity from the fragmentation regions is energy independent. - From Fig. 3 one can conclude that the QGSM favors violation of the Feynman scaling at midrapidity, otherwise the particle density there should not depend on $\sqrt{s}$.

Predictions for the charged particle multiplicity in pp collisions at LHC can also be obtained by the extrapolation of pseudorapidity distributions measured at lower energies. This method [14] relies on the energy independence of the slopes of pseudorapidity spectra combined with logarithmic proportionality to $\sqrt{s}$ of both the width and the height of the distributions. Therefore, any experimental data set from Fig. 3 can be used for the extrapolation, and the results are (see [14])

$$\frac{dN_{NSD}}{d\eta}|_{\eta=0}=4.6\pm0.4 \quad , \quad \frac{dN_{NSD}}{d\eta}|_{\eta=\pm2}=5.25\pm0.7\ .$$

These predictions are a bit lower than the QGSM ones.

One of the consequences of Feynman scaling is the so-called extended longitudinal scaling [15] exhibited by the slopes of (pseudo)rapidity spectra. In the QGSM these slopes are identical in the fragmentation region $y_{beam}\geq -2.5$ as shown in Fig. 4, where the distributions $\frac{1}{\sigma_{NSD}}\frac{d\sigma_{NSD}}{dy}$ are expressed as functions $y-y_{max}$. QGSM indicates that the extended longitudinal scaling remains

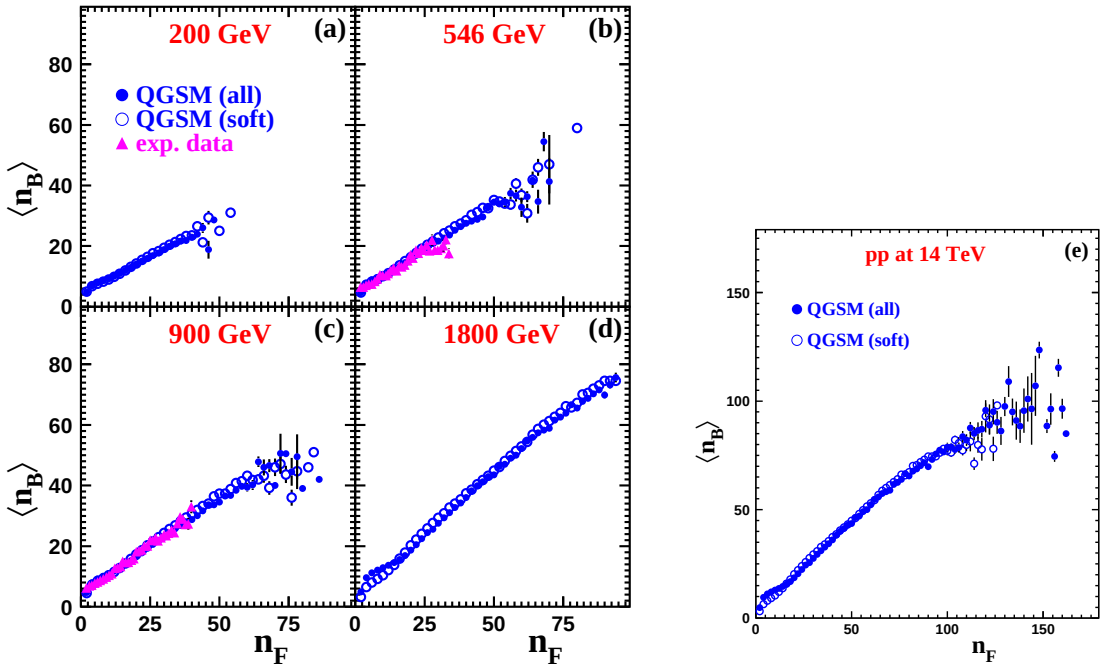

Figure 5: Backward-forward multiplicity dependences $\langle n_B(n_F)\rangle$ for $0 \le |\eta| \le 4$ in non-diffractive pp interactions. Data are taken from [11].

certainly valid at LHC. This result contradicts to the recent prediction based on the statistical thermal model [16]. The latter fits the measured rapidity distributions to the Gaussian, extracts the widths of the Gaussians and implements the energy dependence of the obtained widths to simulate the rapidity spectra at LHC. The extrapolated distribution was found to be much narrower [16] compared to that presented in Fig. 4. We are eagerly awaiting the first LHC measurements of pp collisions to resolve the obvious discrepancy. Note, that experimentally the extended longitudinal scaling was found to hold to 10% in a broad energy range from $\sqrt{s} = 30.8$ GeV to 900 GeV [11].

Correlations between charged particles emitted in forward (F) and backward (B) hemispheres were first observed in [17]. The strength of the correlations is defined as

$$b = \frac{\langle (n_F - \langle n_F \rangle)(n_B - \langle n_B \rangle)\rangle}{[\langle (n_F - \langle n_F \rangle)^2\rangle \langle (n_B - \langle n_B \rangle)^2\rangle]^{1/2}} , \tag{3.3}$$

where n_F and n_B represent multiplicities of charged particles in forward and backward hemispheres, respectively. In Fig. 5 we show the dependence of the mean charged-particle multiplicity in the backward hemisphere $\langle n_B\rangle$, measured in the range $-4 \le \eta \le 0$, on the multiplicity in the forward hemisphere n_F for the symmetric range $0 \le \eta \le 4$ at all energies in question. Comparison with experimental data at $\sqrt{s} = 546$ GeV and 900 GeV shows a good agreement between the model results and the data. This dependence looks pretty linear

$$\langle n_B(n_F)\rangle = a + b\, n_F \ . \tag{3.4}$$

Its slope b increases with energy. In the QGSM the rise of the strength of correlations is linked to increase of number of Pomerons, i.e. strings, with energy in the aforementioned pseudorapidity

range. As one can see from Fig. 5, the correlations between $\langle n_B \rangle$ and n_F are fully determined by soft processes.

4. Conclusions

We see that the quark-gluon model simulations of general characteristics of charged particles in pp collisions, such as pseudorapidy distributions, transverse momentum spectra and backward-forward correlations, at c.m. energies from 200 GeV to 1.8 TeV agree pretty well with the available experimental data. Predictions are made for inelastic and non-single diffractive pp collisions at $\sqrt{s} = 14$ TeV available for the LHC. QGSM predicts violation of Feynman scaling at midrapidity together with its realization in the fragmentation regions. For instance, extended longitudinal scaling is shown to hold at LHC in accord with experimental observations at lower energies. Backward-forward multiplicity correlations are shown to be determined by the soft processes. The correlations will keep its linear dependence $\langle n_B \rangle = a + b n_F$ at LHC as well, and their magnitude b will increase with energy due to rising number of Pomerons.

References

[1] A.B. Kaidalov, *Phys. Lett.* **B116** 459 (1982); A.B. Kaidalov and K.A. Ter-Martirosyan, *Phys. Lett.* **B117**, 247 (1982).

[2] N.S. Amelin and L.V. Bravina, *Sov. J. Nucl. Phys.* **51**, 133 (1990); N.S. Amelin, L.V. Bravina, L.I. Sarycheva, and L.I. Smirnova, *Sov. J. Nucl. Phys.* **51**, 535 (1990).

[3] R. Feynman, *Phys. Rev. Lett.* **23**, 1415 (1969); R. Feynman, *Photon-hadron interactions*, Benjamin, NY 1972.

[4] V. Gribov, *Sov. Phys. JETP* **26**, 414 (1968); L.V. Gribov, E.M. Levin, and M.G. Ryskin, *Phys. Rep.* **100**, 1 (1983).

[5] G. t'Hooft, *Nucl. Phys.* **B72**, 461 (1974).

[6] G. Veneziano, *Phys. Lett.* **B52**, 220 (1974).

[7] M. Baker and K.A. Ter-Martirosyan, *Phys. Rep.* **28C**, 1 (1976); A.B. Kaidalov, *Surveys in High Energy Phys.* **13**, 265 (1999).

[8] M. Cifaloni, G. Marchesini, and G. Veneziano, *Nucl. Phys.* **B98**, 472 (1975).

[9] A. Capella, J. Tran Thanh Van, and J. Kweicinski, *Phys. Rev. Lett.* **58**, 2015 (1987).

[10] R.D. Field and R.P. Feynman, *Nucl. Phys. B* **136**, 1 (1978).

[11] G.J. Alner *et al.* (UA5 Collab.), *Phys. Rep.* **154**, 247 (1987).

[12] F. Abe *et al.* (CDF Collab.), *Phys. Rev. Lett.* **61**, 1819 (1988).

[13] F. Abe *et al.* (CDF Collab.), *Phys. Rev. D* **41**, R2330 (1990).

[14] W. Busza, *J. Phys. G* **35**, 044040 (2008).

[15] G.J. Alner *et al.* (UA5 Collab.), *Z. Phys. C* **33**, 1 (1986).

[16] J. Cleymans, J. Strümpfer, and L. Turko, *Phys. Rev. C* **78**, 017901 (2008).

[17] G.J. Alner *et al.* (UA5 Collab.), *Nucl. Phys. B* **291**, 445 (1987).